Alkali Metal Ions Dictate the Structure and Reactivity of an Iron(II) Imido Complex

Journal:	*Journal of the American Chemical Society*
Manuscript ID	ja-2021-11429e.R1
Manuscript Type:	Article
Date Submitted by the Author:	n/a
Complete List of Authors:	Gao, Yafei; Indiana University Bloomington, Department of Chemistry Pink, Maren; Indiana University System, Molecular Structure Center Smith, Jeremy; Indiana University System, Chemistry

Alkali Metal Ions Dictate the Structure and Reactivity of an Iron(II) Imido Complex

Yafei Gao, Maren Pink, and Jeremy M. Smith*

Department of Chemistry, Indiana University, 800 East Kirkwood Avenue, Bloomington, Indiana 47405, United States

ABSTRACT: The presence of redox innocent metal ions has been proposed to modulate the reactivity of metal ligand multiple bonds, however insight from structure/function relationships is limited. Here, alkali metal reduction of the Fe(III) imido complex [$Ph_2B(^tBuIm)_2Fe$=NDipp] (**1**) provides the series of structurally characterized Fe(II) imido complexes [$Ph_2B(^tBuIm)_2Fe$=NDippLi$(THF)_2$] (**2**), [$Ph_2B(^tBuIm)_2Fe$=NDippNa$(THF)_3$] (**3**), and [$Ph_2B(^tBuIm)_2Fe$=NDippK]$_2$ (**4**), in which the alkali metal cations coordinate the imido ligand. Structural investigations demonstrate that the alkali metal ions modestly lengthen the Fe=N bond distance from that in the charge separated complex [$Ph_2B(^tBuIm)_2Fe$=NDipp][K(18-C-6)THF_2] (**5**), with the longest bond observed for the smallest alkali metal ion. In contrast to **5**, the imido ligands in **2**-**4** can be protonated and alkylated to afford Fe(II) amido complexes. Combined experimental and computational studies reveal that the alkali metal polarizes the Fe=N bond, with the basicity of imido ligand increases according to **5** < **4** ≈ **3** < **2**. The basicity of the imido ligands influences the relative rates of reaction with 1,4-cyclohexadiene, specifically by gating access to complex **5**, which is the species that is active for HAT. All complexes **2**-**4** react with benzophenone form metastable Fe(II) intermediates (**11**-**13**) that subsequently eliminate the metathesis product Ph_2C=NDipp, with relative rates **11** ≈ **12** > **13**. By contrast, the same reaction with **5** does not lead to the formation of Ph_2C=NDipp. These results demonstrate that the coordination of alkali metal ions dictate both the structure and reactivity of the imido ligand, and moreover can direct the reactivity of reaction intermediates.

Introduction

Redox-innocent metal ions have been proposed to modulate the reactivity of intermediates that are at the heart of many biological and chemical oxidation reactions.[1-2] For example, the Ca^{2+} ion is an essential cofactor for water oxidation at the oxygen-evolving center (OEC) of Photosystem II.[3-5] Here, seminal work by Agapie and coworkers on structurally relevant manganese-oxo cubane clusters [MMn_3O_4] (M = Ca^{2+}, Sr^{2+}, Zn^{2+}, Sc^{3+}, Y^{3+}) has demonstrated that these metal ions dramatically impact the redox potentials of the cluster, suggesting a similar role for Ca^{2+} in the OEC.[6-9]

Likewise, studies of model complexes for nonheme iron dioxygenases suggest that the properties of high valent iron oxos are also sensitive to the presence of redox-innocent metal ions.[10] Most notably, Fukuzumi, Nam and coworkers have shown that metal ions such as Mg^{2+}, Zn^{2+}, Sc^{3+} and Ca^{2+} significantly enhance the rate of electron transfer to the model complex [(N4Py)$Fe^{IV}O$]$^{2+}$ (N4Py = *N,N*-bis(2-pyridylmethyl)-*N*-bis(2-pyridyl)methylamine).[11] Moreover, the rate of oxidative dimerization and *N*-demethylation of *N,N*-dimethylanilines is enhanced by Sc^{3+}, while the mechanism of thioanisole oxidation is changed.[12-13] Although the binding of these metal ions to the Fe=O unit is supported by spectroscopic and computational evidence, definitive structural information regarding these interactions is still lacking.[14] While initial crystallographic evidence suggested that Sc^{3+} coordinates to the oxo ligand in [(TMC)$Fe^{IV}O$]$^{2+}$ (TMC = 1,4,8,11-tetramethyl-1,4,8,11-tetraazacyclotetradecane),[15] subsequent computational and experimental studies reveal a more nuanced outcome, with Sc^{3+} coordination accompanied by reduction to Fe^{3+}.[16-17] Moreover, it has also been suggested that redox-innocent metal ions can function as Brönsted acids [$M(H_2O)_n$]$^{m+}$ in the presence of adventitious water, protonating the oxo ligand.[18-19] In the absence of definitive structural characterization, attributing changes in reactivity to the coordination of the redox innocent metal ions can be ambiguous.

While similar effects may be anticipated for imido complexes, even less is known about the impact of redox-innocent metal ions on their reactivity and properties. In one study, Ray and coworkers trapped the transient species $LCu^{II}N$•Ts (L = 3,3′-iminobis(*N*,*N*-dimethylpropylamine), Ts = tosyl) with Sc^{3+}, affording $LCu^{II}N$•(Sc^{3+})Ts, where it was proposed that Sc^{3+} coordinates to Cu^{II}-N unit on the basis of spectroscopic and computational investigations.[20] Whereas ferrocene mediates two electron reduction of $LCu^{II}N$•(Sc^{3+})Ts, in the absence of Sc^{3+} spontaneous one electron reduction of $LCu^{II}N$•Ts to LCu^{II}NHTs is observed. Subsequent work for the series $LCu^{II}N$•(M)Ts (M = Sc^{3+}, Y^{3+}, Eu^{3+}, Ce^{3+}, Zn^{2+}, Ca^{2+}) shows that the spectroscopic properties and nitrene transfer reactions with PPh_3 are independent of M.[21] Thus, the structural effect of the metal cation as well as its relationship to the reactivity of the complex is unclear. While there are scattered examples of structurally characterized metal imido complexes in which a redox innocent metal coordinates the imido ligand,[22-28] the Ce(IV) imidos [($TriNO_x$)CeN(3,5-$(CF_3)_2C_6H_3$)(M$(solv)_n$)] ($TriNO_x$ = Tris(hydroxylaminato) ligand) (M = Li, solv = THF/Et_2O or TMEDA; M = K, Rb, Cs, solv = DME)) are the only complexes for which there is a systematic change in the alkali metal ion.[29-30] However, the impact of the redox-innocent

metal on the reactivity of the imido ligand has not been reported, including comparisons with the chargeseparated imido complex.

We previously reported the synthesis and characterization of the three-coordinate high spin (S = 2) Fe(II) imido complex [$Ph_2B(^tBuIm)_2Fe$=NDipp][K(18-C-6)THF_2].[31] Unusually for a late transition metal complex, the imido ligand is nucleophilic, which enables the catalytic guanylation of carbodiimides under mild conditions. Since this complex is prepared by reduction of the corresponding Fe(III) imido complex, we recognized an opportunity to investigate the properties of congeners with different alkali metal ions. In this contribution, we report the synthesis and characterization of a series of "ate" S = 2 Fe(II) imido complexes [$Ph_2B(^tBuIm)_2Fe$=NDippLi$(THF)_2$] **2**, [$Ph_2B(^tBuIm)_2Fe$=NDippNa$(THF)_3$] **3**, and [$Ph_2B(^tBuIm)_2Fe$=NDippK]$_2$ **4**, in which the alkali metal cations coordinate the imido ligand. Although structural characterization shows modest changes in the bond metrics, both computational and experimental studies reveal that the alkali metal cation can have a dramatic impact on the reactivity of the imido ligand. The cation affects protonation, alkylation, hydrogen atom transfer reactions of the imido complex, as well as the outcome of nucleophilic reactions with benzophenone.

Results and Discussion

Synthesis and Characterization of Imido Complexes with Coordinated Alkali Metals

The green Fe(III) imido complex [$Ph_2B(^tBuIm)_2Fe$=NDipp] (**1**) reacts with 1.2 eq. Li, Na or KC_8 in THF at -78 °C, affording the series of red "ate" high spin (S = 2) Fe(II) imido complexes [$Ph_2B(^tBuIm)_2Fe$=NDippLi$(THF)_2$] (**2**), [$Ph_2B(^tBuIm)_2Fe$=NDippNa$(THF)_3$] (**3**) and [$Ph_2B(^tBuIm)_2Fe$=NDippK]$_2$ (**4**) in 72-81 % yields. Addition of 18-crown-6 sequesters the potassium cation from **4** to provide the previously reported charge separated high spin Fe(II) imido complex [$Ph_2B(^tBuIm)_2Fe$=NDipp][K(18-C-6)THF_2] (**5**) in 79 % yield (Scheme 1).[31]

Complexes **2-4** have been characterized by single crystal X-ray diffraction. While **2** and **3** are monomeric, with the alkali metal ions coordinated by THF solvent, **4** is a dimer[32] where the softer potassium cations interact with the BPh group of the bis(carbene)borate ligand and the Dipp group of the neighboring imido ligand (K···C distances are *ca.* 3.048 to 3.364 Å) (Figure 1). The molecular structures of **2-4** reveal that the imido N atoms are all capped by the respective alkali cations with the M-N distances increasing according to Li < Na < K (Table 1), as expected for their relative ionic radii.[33] By contrast, the Fe-N bond distances follow the order Li > Na > K. These distances are all longer than in **5** (1.777(2) Å), but still 0.1 Å shorter than in three-coordinate Fe(II) amido complexes (*ca.* 1.9 Å).[34] Similar observations are made for the Ce-N bond distance in [($TriNO_x$)CeN(3,5-$(CF_3)_2C_6H_3$)(M$(solv)_n$)] complexes.[30] Together, these Fe-N bond distances suggest that the interaction between alkali cations and imido nitrogen atoms weaken the Fe-N bond, but not at the complete expense of double bond character. Moreover, the relative bond distances indicate that the smaller lithium and sodium cations have a stronger interaction with the imido nitrogen atom than does the potassium cation. In addition to the changes in Fe-N bond distances, the Fe-N-C angles in **2-4** show greater deviation from linearity than for **5** (172.64(19)°), which is in part due to the interaction between the alkali metal ions and the nitrogen atom of the imido ligand. While the iron imido linkage is perturbed by the alkali metal ions, the Fe-C(carbene) bond distances are the same for **2-4** (*ca.* 2.1 Å, see Table 1), although these are slightly longer than for **5**. These distances are comparable with other high spin (S = 2) Fe(II) bis(carbene)borate complexes,[35-37] suggesting that the high spin state in **5** is maintained in **2-4**.

Scheme 1. Synthesis of alkali iron(II) imido complexes **2-4** and charge separated complex **5**.

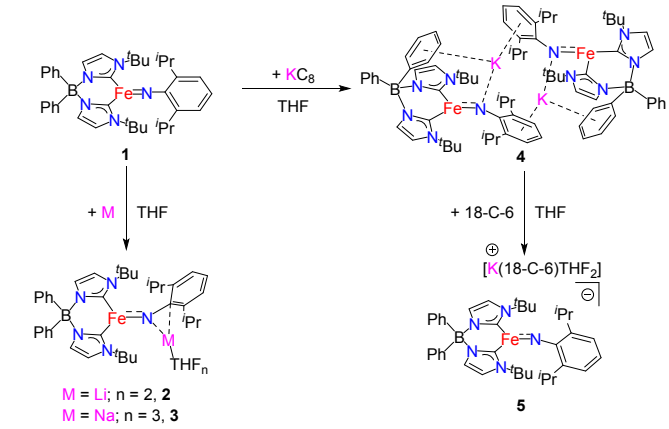

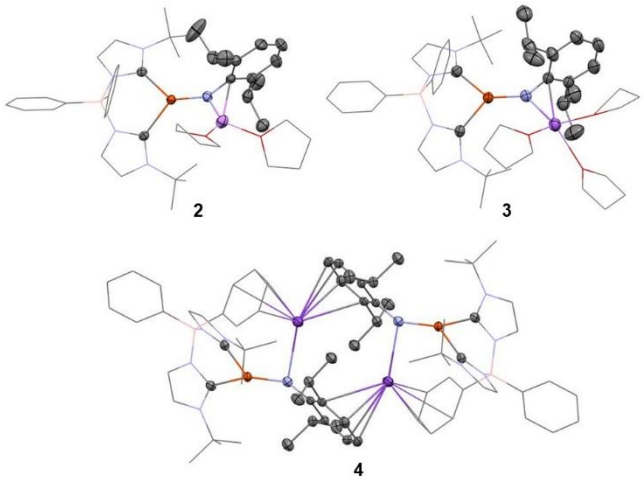

Figure 1. Molecular structures of complexes **2-4**, as determined by single crystal X-ray diffraction. Thermal ellipsoids are shown at 50% probability level, bis(carbene)borate ligands (except for carbene carbon atoms) and coordinating tetrahydrofuran molecules represented as wireframes. Solvent molecules and hydrogen atoms are omitted for clarity. Dark gray, orange, purple and blue ellipsoids represent carbon, iron, alkali metals and nitrogen atoms, respectively.

Table 1. Selected experimental and calculated (B3LYP/def2-SVP/TZVP) parameters for **2-5**.

	2		**3**		**4**		**5**	
	Exp.	Calcd. [c]	Exp.	Calcd. [c]	Exp.	Calcd. [c]	Exp.	Calcd. [31]
Fe-N (imido) (Å)	1.8167(17)	1.829	1.812(2)	1.809	1.793(3)	1.807	1.777(2)	1.779
M···N (imido) (Å) [a]	1.950(4)	1.869	2.440(3)	2.279	2.803(3)	2.644	-	-
Fe-C (Å) [b]	2.110(2)	2.085	2.097(3)	2.081	2.099(4)	2.097	2.084(2)	2.072
Fe-N-C (°)	143.6(1)	132.7	141.5(2)	135.2	145.9(3)	131.6	172.64(19)	147.6

[a] M = Li, Na, or K; [b] Average of the Fe-C(carbene) bond distances; [c] Calculated for the monomeric, solvent free model complexes [$Ph_2B(^tBuIm)_2Fe$=NDipp(M)].

The high spin state assignment is supported by zero-field ^{57}Fe Mössbauer spectroscopy. The 80 K spectra of **2-4** show one doublet with δ = 0.46-0.49 mm/s and $|\Delta E_Q|$ = 1.14-1.45 mm/s. The similarity of these spectral metrics, both with each other and with those for **5** (δ = 0.46 mm/s and $|\Delta E_Q|$ = 1.45 mm/s at 80 K) support the high spin nature of **2-4**. In addition, the similarity of the ^{57}Fe Mössbauer spectral parameters suggests that **2-4** and **5** have similar electronic structures. It is worth noting that the Mössbauer spectrum of **2** has an asymmetric quadrupole doublet at 80 K. This asymmetry is reduced at 220 K, suggesting the onset of slow paramagnetic relaxation at lower temperature.

The ^{1}H NMR spectra of **2-4** are consistent with the structures observed in the solid state. Specifically, ten paramagnetically shifted resonances are observed between -120 and 140 ppm, whose relative integrations allow them to be assigned to protons from the bis(carbene)borate and imido ligands. The chemical shifts for each complex are distinct from each other and from those for the ion-separated complex **5** (Figure S9). The solution magnetic moments, as determined by Evans' method, support the S = 2 formulation for **2** and **3** (*ca.* 5.1 μ_B). In the case of **4**, the magnetic moment (μ_{eff} = 6.3(1) μ_B) is less than the sum of the magnetic moments of two isolated spin-only high spin Fe(II) centers (μ_{eff} = 9.8 μ_B), likely due to antiferromagnetic coupling between the two iron centers. While we cannot definitively exclude the possibility that **4** forms a monomeric structure (akin to **2** and **3**), the distinct ^{1}H NMR spectrum, together the solution magnetic moment and lack of evidence for potassium ion exchange (Figures S10-S11) suggest that the integrity of the solid-state structure is maintained in solution.

Unlike the ^{1}H NMR spectra, the UV-vis spectra of **2-5** are not greatly affected by the alkali cations and show similar absorptions at *ca.* 300 and 320 nm in THF solution (Figure S50). In addition, their electrochemical properties are also similar. The cyclic voltammograms of complexes **3-5** exhibit a reversible anodic wave with $E_{1/2}$ = *ca.* -1.90 V *vs* Fc^+/Fc (Figure S53). In the case of **2**, a reversible anodic wave is observed at a more negative potential ($E_{1/2}$ = -2.03 V), likely due to a greater negative charge on the imido ligand in this complex (see below).

It is notable that complexes **2-4** have greater stability in solution than the charge separated complex **5**. Complete decomposition of **2-4** occurs over 10 days at room temperature in THF-d_8 (0.06 mol/L), compared with only 5 days for **5**. Similarly, **2-4** are stable for over one week in the solid state, by which time **5** has completely decomposed.

Electronic Structure Calculations

Electronic structure calculations were used to assess the impact of the alkali metal ions on the electronic structure of imido complex **5**. To directly compare the effects of the alkali metal ions, a series of THF-free model complexes [$Ph_2B(^tBuIm)_2Fe$=NDipp(M)] (M = Li, **2'**; M = Na, **3'**; M = K, **4'**)[38] were investigated using the electronic structure software ORCA[39] (structural optimization of the full complexes **2** and **3** reveals that the major structural difference is the Fe-N-M angle, see Table S1). Structural optimization (B3LYP/def2-SVP/TZVP) of **2'-4'** provides bond metrics that are similar to those observed for the solid-state structures **2-4** (Table 1), suggesting that solvent and arene interactions involving the alkali metal ions in **2-4** have little effect on the properties of the imido ligand. Furthermore, a series of linear synchronous transit calculations reveal that the longer Fe=N bond lengths and larger Fe-N-C bond angles for **2-4** are due to the alkali metal ions coordinating to the imido ligand **(**Figures S56 and S57**)**. The Fe=N bond length in **2'-4'** increases according to K < Na < Li, following the trend observed for the solid-state structures **2-4**. This suggests that lithium most strongly perturbs the Fe=N bond. However, there is no trend in the calculated Fe-N-C bond angle, and differences with the solid-state structures are likely due to packing forces.

The electronic structures of **2'-4'** are qualitatively similar to that determined for **5**, as reflected by their frontier molecular orbitals (Figures S58-S61). In addition, the Mulliken spin densities on the iron and imido nitrogen atoms in **2'-4'** are similar to those observed for **5** (*ca.* +3.60 and *ca.* +0.20, respectively, see Figures S62-S65). However, the Löwdin Fe=N bond orders in **2'-4'** (1.14-1.19) are lower than in **5** (1.33), as expected for the longer Fe=N bond distances. These bond orders suggest the bond order is close to one, which is also supported by the calculated Wiberg bond indices for these complexes (~0.5, Table S3). Alkali metal ion also decreases the Wiberg bond indices.

The electronic structure calculations provide insight into the impact of the alkali metal ion on the chemical properties of the imido ligand. Analysis of the Fe 3*d* and N 2*p* character in the Fe=N π-bond for **2'-4'** reveals that this orbital is polarized by the alkali metal ion, with the degree of polarization toward imido ligand increasing **2'** > **3'** ≈ **4'** (Figure S66), which is further supported by an NBO analysis, which reveals ~80 %

nitrogen 2*p* orbital character in the Fe=N π bond (Table S3). By comparison, this bond has ~75 % nitrogen 2*p* orbital character in the charge separated complex **5**. Consequently, the Mulliken atomic charges decrease in the order **2'** (-0.99) > **3'** ≈ **4'** (-0.90) > **5** (-0.71). These changes can be rationalized according to a simple molecular orbital interaction diagram for the Fe=NR bond (Figure 2a). Firstly, the alkali metal ions decrease the negative charge on the imido ligand, thereby lowering the energy of imido-based orbitals. Consequently, there is a larger energy difference between this orbital and the appropriate iron-based orbital, which increases the polarization of the resulting molecular orbitals. This polarization is expected to increase the basicity of the imido ligand because the filled imido-based orbitals are at higher energy in the presence of the alkali metal ion (Figure 2b). Secondly, as the Fe-N distance increases in the order **2'** > **3'** ≈ **4'**, the extent of overlap between the iron- and imido-based orbitals decreases. This increases the relative energy of the filled imido-based orbitals. Thus, the basicity of the imido ligand is expected to increase in the order **2' > 3' ≈ 4'** (Figure 2b).

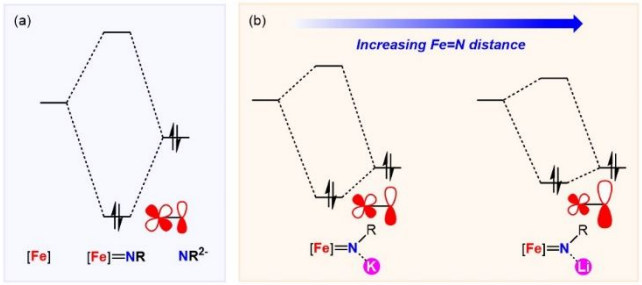

Figure 2. Qualitative MO diagrams illustrating the effect of the alkali metal ion on the Fe=N orbital interaction.

In summary, the electronic structure calculations reveal that coordination of the alkali metal ions perturbs the iron-imido orbital interaction by both polarizing the Fe=N bond and decreasing orbital overlap. Based on the combination of these factors, the basicity of the imido ligands is expected to decrease in the order **2** > **3** ≈ **4** > **5**.

Protonation and Alkylation Reactions

Protonation and alkylation reactions support the basic character of the imido ligand in **2-4**, as suggested by the electronic structure calculations. Moreover, these experiments reveal that the alkali metal ions provide access to reaction pathways that are inaccessible in their absence.

Complexes **2-4** react smoothly with 1 eq. [LutH][Cl] (relative to Fe) in THF at -78 °C, yielding the yellow Fe(II) amido complex [$Ph_2B(^tBuIm)_2FeNHDipp$] (**6**) in 79-82 % yields (Scheme 2). The molecular structure of **6** (Figure 3), as determined by single crystal X-ray diffraction, reveals a trigonal-planar iron center (sum of angles = 359°) with an Fe-N bond distance (1.917(1) Å) that is comparable to other three-coordinate Fe(II) amido complexes.[34] The complex was also characterized in solution ^{1}H NMR spectroscopy and magnetometry, confirming **6** as a high spin (S = 2) Fe(II) amido complex. The spin state assignment was further supported by zero-field ^{57}Fe Mössbauer spectroscopy, with spectral parameters (δ = 0.47 mm/s and $|\Delta E_Q|$ = 1.39 mm/s at 80 K) that are consistent with other three-coordinate high spin Fe(II) complexes.[37, 40-41]

The imido nitrogen atom in **2-4** can also be alkylated. As with protonation, complexes **2-4** react smoothly with 1 eq. $PhCH_2Br$ (relative to Fe) at -78 °C to afford the yellow Fe(II) amido complex [$Ph_2B(^tBuIm)_2FeN(CH_2Ph)Dipp$] (**7**) in 77-86% yields (Scheme 2). The molecular structure of **7** has also been determined by single crystal X-ray diffraction (Figure 3). As with **6**, the iron center is trigonal-planar (sum of angles = 360 °) with a similar Fe-N bond distance (1.901(3) Å). The complex has been characterized in solution by ^{1}H NMR spectroscopy and magnetometry, with the S = 2 spin state further supported by zero-field ^{57}Fe Mössbauer spectroscopy (δ = 0.52 mm/s and $|\Delta E_Q|$ = 1.14 mm/s at 80 K).

Scheme 2. Reactions of **2-4** with [LutH][Cl] and $PhCH_2Br$.

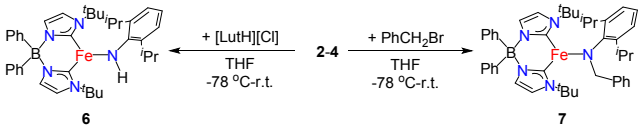

6 7

Although nucleophilic iron imido complexes have been isolated,[42-47] to the best of our knowledge, reactions with Brönsted acids have not been previously reported. Similarly, we are unaware of alkylation reactions using organic halides for any transition metal imido complex.

Interestingly, divergent results are obtained for analogous reactions with the charge separated complex **5**. Reaction with [LutH][Cl] is intractable, and no detectable concentrations of amido complex **6** are formed. While the reduction potential of [LutH][Cl] does not definitively exclude an alternate mechanism involving outer-sphere electron transfer (Figures S54), it is notable that complex **1** and H_2 are not observed. Similarly, the reaction of **5** with $PhCH_2Br$ provides a multitude of unknown products, although trace **7** is observed. In this case, outer sphere electron transfer is unlikely due to the significantly more cathodic reduction potential for $PhCH_2Br$ (Figure S55). The difference in reaction outcomes for complexes **2-4** and **5** points to critical role for the alkali cation in controlling the reactivity of the imido ligand. The ability to protonate and alkylate the imido ligand in complexes **2-4** but not **5** may have relevance in the context of N_2 functionalization. It is worth noting that that alkali metal additives are important in industrial NH_3 synthesis.[48]

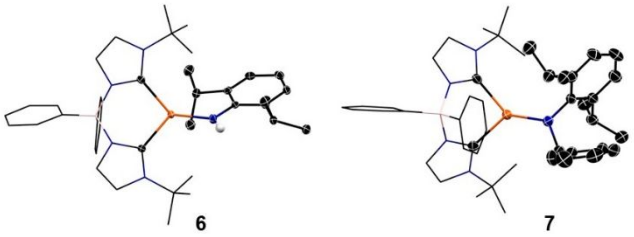

Figure 3. Molecular structures of complexes **6** and **7**, as determined by single crystal X-ray diffraction. Thermal ellipsoids are shown at 50% probability level, bis(carbene)borate ligands (except for carbene carbon atoms) represented as wireframes. Solvent molecules and most hydrogen atoms are omitted for clarity. Dark gray, light gray, orange, and blue ellipsoids represent carbon, hydrogen, iron and nitrogen atoms, respectively.

While protonation of **2-4** with [LutH][Cl] is irreversible, the weaker acid H_2NDipp establishes an equilibrium with the previously reported bis(anilido) complex **8** (Scheme 3).[31] Here K_{eq} is observed to gradually decrease in the order **5** > **4** > **3** ≈ **2**. Importantly, the formulation of **8** is independent of the alkali metal ion, as demonstrated by spectroscopic properties that are identical in all cases (Figures S14-S16). These results experimentally validate the computational predictions of the relative basicities for the imido ligand in **2-5**.

Scheme 3. Equilibrium reaction involving **8** with **2-5** and $DippNH_2$.

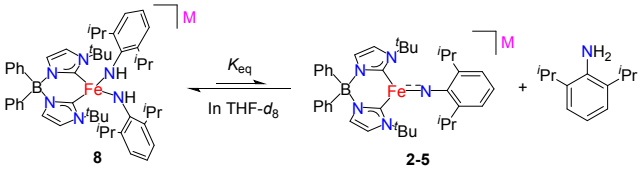

M	[K(18-C-6)]	K	Na	Li
K_{eq} (×10^{-3} mol/L)	8.0(3)	6.2(3)	2.3(6)	1.9(1)

Hydrogen Atom Transfer

Iron imido complexes are known to participate in hydrogen atom transfer (HAT) reactions, although this reactivity has only been reported for complexes in the Fe(III)[43-44, 49-57], Fe(IV)[46, 58-59] and Fe(V)[60] oxidation states, and not for Fe(II)[47, 61-63]. Nonetheless, since the electronic structures of **2-4** (and **5**) reveal radical character on the imido nitrogen (Figures S62-S65), we hypothesized that these complexes may be active in HAT reactions.

The room temperature reaction of **5** with 0.5 eq. 1,4-cyclohexadiene (gas phase BDFE = 67.8 kcal/mol)[64] in THF-d_8 results in the stoichiometric formation of benzene over the course of a few minutes, along a spectroscopically-characterized iron complex that we tentatively propose to be the three-coordinate high spin (S = 3/2) Fe(I) anilido complex $[Ph_2B(^tBuIm)_2FeNHDipp][K(18\text{-C-6})THF_2]$ (**9-[K(18-C-6)]**) (Scheme 4). Although the thermal instability of **9-[K(18-C-6)]** prevented its characterization by single crystal X-ray diffraction, its ^{57}Fe Mössbauer spectral parameters (δ = 0.64 mm/s and $|\Delta E_Q|$ = 2.95 mm/s at 80 K) are similar to those reported for other S = 3/2 three-coordinate Fe(I) complexes.[65-66] Complex **9-[K(18-C-6)]** decomposes over the course of a few hours to afford the previously reported bis(anilido) Fe(II) complex $[Ph_2B(^tBuIm)_2Fe(NHDipp)_2][K(18\text{-C-6})THF_2]$ (**8-[K(18-C-6)]**),[31] as characterized by ^{1}H NMR spectroscopy (Scheme 4). The fate of the remaining iron is unknown. No other paramagnetic complexes are observed by ^{1}H NMR spectroscopy and attempts to trap the Fe(0) complex expected from the disproportionation of **9-[K(18-C-6)]** were unsuccessful.

Scheme 4. Reactions of **2-5** with 1,4-cyclohexadiene.

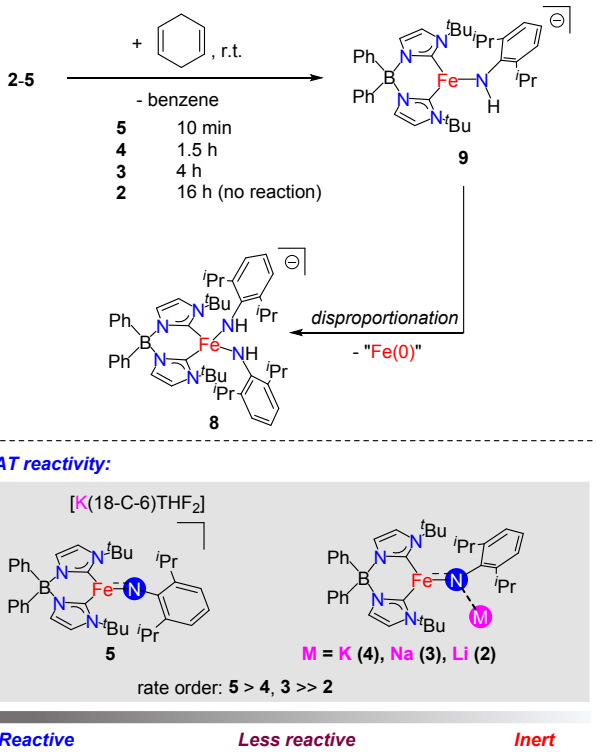

The outcome of the reactions between **2-4** and 1,4-cyclohexadiene depends on the nature of the alkali metal. Complexes **3** and **4** also react with 1,4-cyclohexadiene, ultimately yielding the Fe(II) bis(anilido) complex $[Ph_2B(^tBuIm)_2Fe(NHDipp)_2]$ (**8**) along with stoichiometric benzene (Scheme 4). However, these reactions are significantly slower than for **5**, requiring 1.5 and 4 hours for the full consumption of **4** and **3**, respectively (Figures S21-S22). By contrast, complex **2** shows no evidence for reaction with 1,4-cyclohexadiene, even after 16 hours under the same conditions (Figure S23). While the reaction with **5** was too fast to measure, we were able to determine the kinetic isotope effect for the reactions of **3** and **4** with 1,4-cyclohexadiene (see SI for details). It is notable that the same KIE is observed for these two imido complexes (k_H/k_D = 4.8). This supports a mechanism in which HAT from the 1,4-cyclohexadiene to **3** or **4** involves the same iron imido intermediate.

The alkali metal ion also dictates the ability of the imido ligand to abstract hydrogen atoms from C-H bonds, as determined by the C-H bond strength. Thus, **5** reacts with toluene (gas phase BDFE = 81.6 kcal/mol)[64] over the course of several hours (Figure S24) to afford **8-[K(18-C-6)]**. By contrast,

complexes **2-4** are inert towards toluene, with only a minor conversion observed over 2 d for the most reactive complex **4** (Figure S25). The KIE for the reaction of **5** with toluene (k_H/k_D = 6.4) is also consistent with a mechanism involving HAT.

The differences in reactivity demonstrate the profound impact of the alkali metal on the activity of the Fe=N unit in HAT. Thus, the rate of reaction with 1,4-cyclohexadiene is fastest for the alkali free imido complex **5**, with the rate for **2-4** decreasing in the order **4** > **3** >> **2**. In addition, only complex **5** shows appreciable reactivity towards toluene. These rate differences are unlikely to stem from thermodynamic factors. Notably, the relative rates are opposite to the basicity trends for **2-5** (see above). Moreover, DFT estimates for the gas phase $BDFE_{N-H}$ in **9** show that this value is largely insensitive to the alkali metal ion (62-65 kcal/mol in the presence of alkali metal ions and 66 kcal/mol in their absence).[67] Additionally, since the rate decreases as the ionic radius of the alkali metal ion decreases, the relative rates are unlikely to result from steric effects. We note that steric effects have been invoked in the context of N_2 cleavage by low coordinate iron complexes, specifically by controlling access to the N_2 ligand.[68] Together, this suggests that HAT from 1,4-cyclohexadiene to **2-5** is largely kinetically controlled. To account for the observed relative rates, we propose that only complex **5** is capable of HAT. The coordinating alkali metal ions in **2-4** render the imido nitrogen atom inaccessible. Therefore, cleavage of the M···N(imido) bond in **2-4** is required for the HAT reaction to occur (Scheme 5, shown for 1,4-cyclohexadiene). More basic imido ligands will have stronger interactions with the alkali metal ion in **2-4**, reducing the concentration of active complex **5**, as measured by K_{eq}' in Scheme 5. Thus, the relative basicity of the imido ligand in **2-4** is important for the relative rate of HAT since it determines the magnitude of K_{eq}'. Reaction of **2** with 1,4-cyclohexadiene is inhibited due to the very strong interaction between the small Li^+ ion and basic imido ligand. This hypothesis is supported by the calculated gas phase interaction energies between the imido ligand and alkali cations which follow the order Li > Na > K (Scheme 5).

Scheme 5. Proposed pathway for HAT requires cleavage of the M···N(imido) bond in **2-4.** Calculated gas phase interaction energies between the imido complex and alkali cations (298 K).

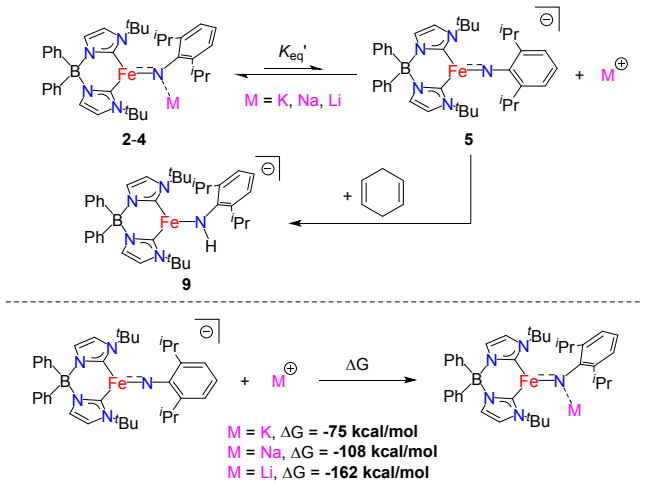

Nucleophilic Reactions with Benzophenone: Double Bond Metathesis

While less common than for early metal imido complexes, a number of iron imido complexes have been reported to react as nucleophiles with unsaturated substrates in [2+2] reactions.[31, 46] We previously reported on [2+2] reactions between **5** and carbodiimides, which provides the basis for the catalytic guanylation of carbodiimides.[31] Since ketones are known to be substrates for [2+2] reactions,[30, 69] we hypothesized that alkali cations would impact the reactivity of Fe(II) imido complexes **2-4** and **5** with benzophenone, specifically by interactions with the oxygen atom.

Scheme 6. Reactions of **2-5** with benzophenone.

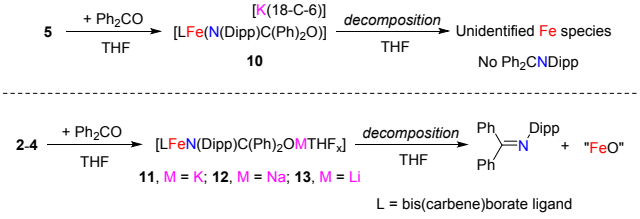

Reaction of **5** with 1 eq. benzophenone quickly forms a new purple paramagnetic species. This is tentatively proposed to be the intermediate that results from nucleophilic attack on Ph_2CO, $[Ph_2B(^tBuIm)_2Fe(N(Dipp)C(Ph)_2O)][K(18\text{-}C\text{-}6)]$ (**10**) on the basis of spectroscopic characterization (Scheme 6, Figures S26 and S42). A single iron-containing species is observed in ^{57}Fe Mössbauer spectrum, with parameters (δ = 0.46 mm/s and $|\Delta E_Q|$ = 2.13 mm/s at 80 K) that are consistent with S = 2 Fe(II). We note that similar reaction of **5** with the carbodiimide ^{i}PrN=C=N^{i}Pr provides the structurally and spectroscopically guanidinate product that is formed *via* a [2+2] cycloaddition reaction.[31] Complex **10** decomposes over several hours to afford multiple unknown iron products, along with trace amounts of the imine Ph_2C=NDipp (Figure S26). This thermal instability has hindered attempts to characterize this complex by single crystal X-ray diffraction.

By contrast, reaction of 1 eq. benzophenone (relative to Fe) with **4** results in the immediate formation of a brown solution. The resulting ^1H NMR spectrum reveals the formation of a new paramagnetic species, which is proposed to be $[Ph_2B(^tBuIm)_2FeN(Dipp)C(Ph)_2OK(THF)_x]$ (**11**) (Figure S27). However, the spectrum of **11** differs from that observed for **10**. The ^{57}Fe Mössbauer spectrum of **11** also reveals a single iron-containing complex that has similar spectral parameters to those observed for **10** (δ = 0.44 mm/s and $|\Delta E_Q|$ = 1.38 mm/s at 80 K). It is worth nothing that these spectral parameters are the same as three-coordinate amido complexes **6** and **7**. Addition of 18-crown-6 to **11** provides **10**, revealing that these complexes are structurally related. Complexes **3** and **2** also react with 1 eq. benzophenone to produce new paramagnetic iron complexes **12** and **13**, respectively. Interestingly, the isomer shift for these complexes decreases in the order **11** > **12** > **13**, suggesting that the alkali metal ions withdraw electron density from iron according to their relative electronegativities. As with **10**, the thermal instability of these complexes has hindered attempts to obtain single crystal X-ray diffraction data.

In contrast to **10**, complexes **11-13** decompose over hours to provide the imine Ph_2C=NDipp (62 % isolated yield, Figures S27-S29). Based on a combination of spectroscopic and reactivity studies, we tentatively suggest the concomitant formation of iron oxo complex(es) (See SI for details). Therefore, complexes **2-4** react with benzophenone to afford the double bond metathesis product Ph_2C=NDipp. A similar double bond metathesis has also been observed in the reaction of "ate" phosphinidene complex [(PNP)Sc(μ_2-P[DMP])(μ_2-Br)Li] (PNP = N[2-P($CHMe_2$)$_2$-4-methylphenyl]$^{2-}$) (DMP = 2,6-$Mes_2C_6H_3$) with benzophenone, which provides the phosphaalkene Ph_2C=P[DMP] along with putative "(PNP)ScO".[69]

Interestingly, **11-13** decompose with rates that depend on the alkali metal ion. Kinetic measurements reveal first-order decomposition for **11-13**, with k_{obs} (**11**) ≈ k_{obs}(**12**) > k_{obs}(**13**) (Figure 4). Thus, the alkali metal ion plays a critical role in stabilizing the intermediates **11-13**. Together with the fact that imine elimination is not a major decomposition pathway for **10**, our observations reveal that the imine elimination step is dictated by electrostatic interactions. Thus, the most Lewis acidic lithium cation is the best at intermediate **13**, leading to a slower rate of imine elimination for **13**. All three alkali metal cations provide a driving force for the reaction by stabilizing the proposed iron oxo complex. In the case of complex **10**, Ph_2C=NDipp is not formed as the sequestered alkali metal cation cannot stabilize the iron oxo coproduct.

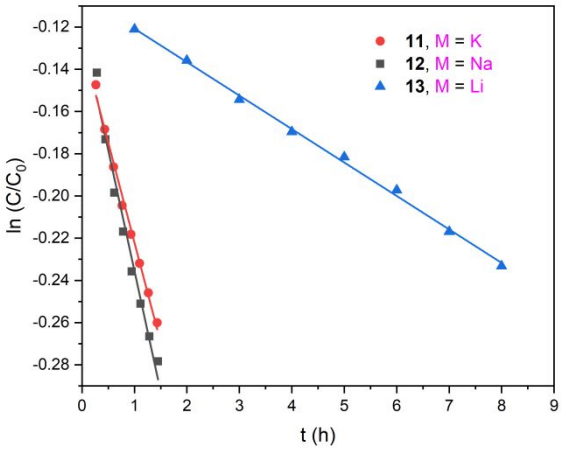

Figure 4. Kinetic traces for the decomposition of **11-13**. For **11** (M = K), **12** (M = Na) and **13** (M = Li), the k_{obs} are 0.090 h^{-1}, 0.115 h^{-1} and 0.016 h^{-1}, respectively. C_0 represents the initial concentration of **11-13**.

Conclusions

The series of structurally and spectroscopically characterized complexes **2-4** provide insight into effect of the alkali metal ion on both the structure and reactivity of the iron imido unit. Structurally, the alkali metal ions lead to a modest elongation of the Fe-N bond distance in the order **2** > **3** ≈ **4**. These distances are all longer than in the charge separated imido complex **5**.

Despite the modest changes in bond metrics, the alkali metal ion has an impact on the reactivity of the imido ligand. Computational and experimental results reveal that the alkali metal ion modifies the basicity of the imido nitrogen atom by further polarizing the Fe=N bond. The imido ligand in the charge separated complex **5** is the least basic, with the basicity gradually increasing in the order **5** < **4** ≈ **3** < **2**. Increasing the Fe-N bond length increases the negative charge density on the imido nitrogen atom.

The interaction between the basic imido ligand and the alkali metal controls the relative rate of HAT from 1,4-cyclohexadiene. The rate of reaction decreases in the order **5** > **4** ≈ **3** >> **2**, with complete inhibition of the reaction for **2**. Here, the alkali metal ions kinetically control the reaction by gating access to the imido complex that is active for HAT.

Although all the imido complexes **2-5** react rapidly with benzophenone afford metastable Fe(II) amido intermediates **10** and **11-13**, respectively, the alkali metal ions are key to the subsequent chemistry. Thus, the rate of decomposition for **11-13** follows the order **11** ≈ **12** > **13**, in all cases providing the metathesis product Ph_2C=NDipp along with a putative iron oxo species. By contrast, only trace Ph_2C=NDipp is formed from **10**, demonstrating the importance of the alkali metal in directing the reactivity of the intermediate species. The different outcomes for the protonation and alkylation **2-4** and **5** similarly demonstrate the ability of the alkali metal ion to direct the course of the reaction.

In summary, we find that coordinated alkali metal ions direct the reactivity of imido complexes through impacts on both the ground state and reaction intermediates. While the structural impact on the iron imido unit appears to be relatively modest, as quantified by metrical changes, the alkali metal ions have a dramatic effect on the rates and pathways of reaction. The alkali metal ions therefore provide a mechanism for tuning the reactivity of the imido ligand, where the extremes of reactivity are observed for **2**, which contains the most Lewis acidic alkali metal ion, and the charge separated complex **5**.

ASSOCIATED CONTENT

Supporting Information. Full experimental and computational details. This material is available free of charge via the Internet at http://pubs.acs.org.

AUTHOR INFORMATION

Corresponding Author

* Jeremy M. Smith. E-mail: smith962@indiana.edu.

Notes

The authors declare no competing financial interest.

ACKNOWLEDGMENT

This material is based upon work supported by the U.S. Department of Energy, Office of Science, Office of Basic Energy Sciences under Award Number DE-SC0019466. Support for the acquisition of the Bruker Venture D8 diffractometer through the Major Scientific Research Equipment Fund from the President of Indiana University and the Office of the Vice President for Research is gratefully acknowledged

REFERENCES

(1) Fukuzumi, S.; Ohkubo, K. Metal Ion-Coupled and Decoupled Electron Transfer. *Coord. Chem. Rev.* **2010**, *254*, 372-385.

(2) Fukuzumi, S.; Ohkubo, K.; Lee, Y. M.; Nam, W. Lewis Acid Coupled Electron Transfer of Metal-Oxygen Intermediates. *Chem. Eur. J.* **2015**, *21*, 17548-17559.

(3) McEvoy, J. P.; Brudvig, G. W. Water-Splitting Chemistry of Photosystem II. *Chem. Rev.* **2006**, *106*, 4455-4483.

(4) Yocum, C. F. The Calcium and Chloride Requirements of the O_2 Evolving Complex. *Coord. Chem. Rev.* **2008**, *252*, 296-305.

(5) Yachandra, V. K.; Yano, J. Calcium in the Oxygen-Evolving Complex: Structural and Mechanistic Role Determined by X-Ray Spectroscopy. *J. Photochem. Photobiol. B: Biol.* **2011**, *104*, 51-59.

(6) Kanady, J. S.; Tsui, E. Y.; Day, M. W.; Agapie, T. A Synthetic Model of the Mn_3Ca Subsite of the Oxygen-Evolving Complex in Photosystem II. *Science* **2011**, *333*, 733-736.

(7) Tsui, E. Y.; Agapie, T. Reduction Potentials of Heterometallic Manganese-Oxido Cubane Complexes Modulated by Redox-Inactive Metals. *Proc. Natl. Acad. Sci. U.S.A.* **2013**, *110*, 10084-10088.

(8) Tsui, E. Y.; Kanady, J. S.; Agapie, T. Synthetic Cluster Models of Biological and Heterogeneous Manganese Catalysts for O_2 Evolution. *Inorg. Chem.* **2013**, *52*, 13833-13848.

(9) Tsui, E. Y.; Tran, R.; Yano, J.; Agapie, T. Redox-Inactive Metals Modulate the Reduction Potential in Heterometallic Manganese-Oxido Clusters. *Nat. Chem.* **2013**, *5*, 293-299.

(10) Lee, J. L.; Ross, D. L.; Barman, S. K.; Ziller, J. W.; Borovik, A. S. C-H Bond Cleavage by Bioinspired Nonheme Metal Complexes. *Inorg. Chem.* **2021**, *60*, 13759-13783.

(11) Morimoto, Y.; Kotani, H.; Park, J.; Lee, Y. M.; Nam, W.; Fukuzumi, S. Metal Ion-Coupled Electron Transfer of a Nonheme Oxoiron(IV) Complex: Remarkable Enhancement of Electron-Transfer Rates by Sc^{3+}. *J. Am. Chem. Soc.* **2011**, *133*, 403-405.

(12) Park, J.; Morimoto, Y.; Lee, Y. M.; Nam, W.; Fukuzumi, S. Metal Ion Effect on the Switch of Mechanism from Direct Oxygen Transfer to Metal Ion-Coupled Electron Transfer in the Sulfoxidation of Thioanisoles by a Non-Heme Iron(IV)-Oxo Complex. *J. Am. Chem. Soc.* **2011**, *133*, 5236-5239.

(13) Park, J.; Morimoto, Y.; Lee, Y. M.; You, Y.; Nam, W.; Fukuzumi, S. Scandium Ion-Enhanced Oxidative Dimerization and N-Demethylation of N,N-Dimethylanilines by a Non-Heme Iron(IV)-Oxo Complex. *Inorg. Chem.* **2011**, *50*, 11612-11622.

(14) Oswald, V. F.; Lee, J. L.; Biswas, S.; Weitz, A. C.; Mittra, K.; Fan, R.; Li, J.; Zhao, J.; Hu, M. Y.; Alp, E. E.; Bominaar, E. L.; Guo, Y.; Green, M. T.; Hendrich, M. P.; Borovik, A. S. Effects of Noncovalent Interactions on High-Spin Fe(IV)-Oxido Complexes. *J. Am. Chem. Soc.* **2020**, *142*, 11804-11817.

(15) Fukuzumi, S.; Morimoto, Y.; Kotani, H.; Naumov, P.; Lee, Y. M.; Nam, W. Crystal Structure of a Metal Ion-Bound Oxoiron(IV) Complex and Implications for Biological Electron Transfer. *Nat. Chem.* **2010**, *2*, 756-759.

(16) Swart, M. A Change in the Oxidation State of Iron: Scandium is not Innocent. *Chem. Commun.* **2013**, *49*, 6650-6652.

(17) Prakash, J.; Rohde, G. T.; Meier, K. K.; Jasniewski, A. J.; Van Heuvelen, K. M.; Munck, E.; Que, L., Jr. Spectroscopic Identification of an Fe^{III} Center, not Fe^{IV}, in the Crystalline Sc-O-Fe Adduct Derived from $[Fe^{IV}(O)(TMC)]^{2+}$. *J. Am. Chem. Soc.* **2015**, *137*, 3478-3481.

(18) Sankaralingam, M.; Lee, Y. M.; Karmalkar, D. G.; Nam, W.; Fukuzumi, S. A Mononuclear Non-heme Manganese(III)-Aqua Complex as a New Active Oxidant in Hydrogen Atom Transfer Reactions. *J. Am. Chem. Soc.* **2018**, *140*, 12695-12699.

(19) Rice, D. B.; Grotemeyer, E. N.; Donovan, A. M.; Jackson, T. A. Effect of Lewis Acids on the Structure and Reactivity of a Mononuclear Hydroxomanganese(III) Complex. *Inorg. Chem.* **2020**, *59*, 2689-2700.

(20) Kundu, S.; Miceli, E.; Farquhar, E.; Pfaff, F. F.; Kuhlmann, U.; Hildebrandt, P.; Braun, B.; Greco, C.; Ray, K. Lewis Acid Trapping of an Elusive Copper-Tosylnitrene Intermediate Using Scandium Triflate. *J. Am. Chem. Soc.* **2012**, *134*, 14710-14713.

(21) Monte-Pérez, I.; Kundu, S.; Ray, K. An Open-Shell Spin Singlet Copper-Nitrene Intermediate Binding Redox-innocent Metal Ions: Influence of the Lewis Acidity of the Metal Ions on Spectroscopic and Reactivity Properties. *Z. Anorg. Allg. Chem.* **2015**, *641*, 78-82.

(22) Scott, J.; Basuli, F.; Fout, A. R.; Huffman, J. C.; Mindiola, D. J. Evidence for the Existence of a Terminal Imidoscandium Compound: Intermolecular C-H Activation and Complexation Reactions with the Transient Sc=NAr Species. *Angew. Chem. Int. Ed.* **2008**, *47*, 8502-8505.

(23) Wright, W. R.; Batsanov, A. S.; Howard, J. A.; Tooze, R. P.; Hanton, M. J.; Dyer, P. W. Exploring the Reactivity of Tungsten Bis(imido) Dimethyl Complexes with Methyl Aluminium Reagents: Implications for Ethylene Dimerization. *Dalton. Trans.* **2010**, *39*, 7038-7045.

(24) Schwarz, A. D.; Nielson, A. J.; Kaltsoyannis, N.; Mountford, P. The First Group 4 Metal Bis(imido) and Tris(imido) Complexes. *Chem. Sci.* **2012**, *3*, 819-824.

(25) Wright, W. R.; Batsanov, A. S.; Messinis, A. M.; Howard, J. A.; Tooze, R. P.; Hanton, M. J.; Dyer, P. W. Application of Molybdenum Bis(imido) Complexes in Ethylene Dimerisation Catalysis. *Dalton. Trans.* **2012**, *41*, 5502-5511.

(26) Akagi, F.; Suzuki, S.; Ishida, Y.; Hatanaka, T.; Matsuo, T.; Kawaguchi, H. Reactions of a Niobium Nitride Complex Prepared from Dinitrogen: Synthesis of Imide and Ureate Complexes and Ammonia Formation. *Eur. J. Inorg. Chem.* **2013**, *2013*, 3930-3936.

(27) Mullane, K. C.; Lewis, A. J.; Yin, H.; Carroll, P. J.; Schelter, E. J. Anomalous One-Electron Processes in the Chemistry of Uranium Nitrogen Multiple Bonds. *Inorg. Chem.* **2014**, *53*, 9129-9139.

(28) Anderson, N. H.; Xie, J.; Ray, D.; Zeller, M.; Gagliardi, L.; Bart, S. C. Elucidating Bonding Preferences in Tetrakis(imido)uranate(VI) Dianions. *Nat. Chem.* **2017**, *9*, 850-855.

(29) Solola, L. A.; Zabula, A. V.; Dorfner, W. L.; Manor, B. C.; Carroll, P. J.; Schelter, E. J. An Alkali Metal-Capped Cerium(IV) Imido Complex. *J. Am. Chem. Soc.* **2016**, *138*, 6928-6931.

(30) Solola, L. A.; Zabula, A. V.; Dorfner, W. L.; Manor, B. C.; Carroll, P. J.; Schelter, E. J. Cerium(IV) Imido Complexes: Structural, Computational, and Reactivity Studies. *J. Am. Chem. Soc.* **2017**, *139*, 2435-2442.

(31) Gao, Y.; Carta, V.; Pink, M.; Smith, J. M. Catalytic Carbodiimide Guanylation by a Nucleophilic, High Spin Iron(II) Imido Complex. *J. Am. Chem. Soc.* **2021**, *143*, 5324-5329.

(32) Complex **4** crystallizes with two independent molecules in the asymmetric unit. Since the only significant difference is the Fe-N-C angle, only one molecule will be discussed.

(33) Shannon, R. D. Revised Effective Ionic Radii and Systematic Studies of Interatomic Distances in Halides and Chalcogenides. *Acta Cryst.* **1976**, *A32*, 751-767.

(34) Wang, X.; Mo, Z.; Xiao, J.; Deng, L. Monomeric Bis(anilido)iron(II) Complexes with N-Heterocyclic Carbene

Ligation: Synthesis, Characterization, and Redox Reactivity Toward Aryl Halides. *Inorg. Chem.* **2013**, *52*, 59-65.
(35) Hickey, A. K.; Lee, W. T.; Chen, C. H.; Pink, M.; Smith, J. M. A Bidentate Carbene Ligand Stabilizes a Low-Coordinate Iron(0) Carbonyl Complex. *Organometallics* **2016**, *35*, 3069-3073.
(36) Hickey, A. K.; Greer, S. M.; Valdez-Moreira, J. A.; Lutz, S. A.; Pink, M.; DeGayner, J. A.; Harris, T. D.; Hill, S.; Telser, J.; Smith, J. M. A Dimeric Hydride-Bridged Complex with Geometrically Distinct Iron Centers Giving Rise to an S = 3 Ground State. *J. Am. Chem. Soc.* **2019**, *141*, 11970-11975.
(37) Lutz, S. A.; Hickey, A. K.; Gao, Y.; Chen, C. H.; Smith, J. M. Two-State Reactivity in Iron-Catalyzed Alkene Isomerization Confers *σ*-Base Resistance. *J. Am. Chem. Soc.* **2020**, *142*, 15527-15535.
(38) The structural metrics with THF are similar, see SI, Table S1.
(39) Neese, F. Software Update: The ORCA Program System, Version 4.0. *Wiley Interdiscip. Rev.: Comput. Mol. Sci.* **2018**, *8*, No. e1327.
(40) Andres, H.; Bominaar, E. L.; Smith, J. M.; Eckert, N. A.; Holland, P. L.; Munck, E. Planar Three-Coordinate High-Spin Fe^{II} Complexes with Large Orbital Angular Momentum: Mossbauer, Electron Paramagnetic Resonance, and Electronic Structure Studies. *J. Am. Chem. Soc.* **2002**, *124*, 3012-3025.
(41) Liu, Y.; Wang, L.; Deng, L. Three-Coordinate Iron(II) Dialkenyl Compound with NHC Ligation: Synthesis, Structure, and Reactivity. *Organometallics* **2015**, *34*, 4401-4407.
(42) Brown, S. D.; Betley, T. A.; Peters, J. C. A Low-Spin d5 Iron Imide: Nitrene Capture by Low-Coordinate Iron(I) Provides the 4-Coordinate Fe(III) Complex $[PhB(CH_2PPh_2)_3]FeN$-*p*-tolyl. *J. Am. Chem. Soc.* **2003**, *125*, 322-323.
(43) Eckert, N. A.; Vaddadi, S.; Stoian, S.; Lachicotte, R. J.; Cundari, T. R.; Holland, P. L. Coordination-Number Dependence of Reactivityin an Imidoiron(III) Complex. *Angew. Chem. Int. Ed.* **2006**, *45*, 6868 –6871.
(44) Cowley, R. E.; Eckert, N. A.; Vaddadi, S.; Figg, T. M.; Cundari, T. R.; Holland, P. L. Selectivity and Mechanism of Hydrogen Atom Transfer by an Isolable Imidoiron(III) Complex. *J. Am. Chem. Soc.* **2011**, *133*, 9796-9811.
(45) Zhang, H.; Ouyang, Z.; Liu, Y.; Zhang, Q.; Wang, L.; Deng, L. (Aminocarbene)(divinyltetramethyldisiloxane)iron(0) Compounds: A Class of Low-Coordinate Iron(0) Reagents. *Angew. Chem. Int. Ed.* **2014**, *53*, 8432-8436.
(46) Wang, L.; Hu, L.; Zhang, H.; Chen, H.; Deng, L. Three-Coordinate Iron(IV) Bisimido Complexes with Aminocarbene Ligation: Synthesis, Structure, and Reactivity. *J. Am. Chem. Soc.* **2015**, *137*, 14196-14207.
(47) Cheng, J.; Liu, J.; Leng, X.; Lohmiller, T.; Schnegg, A.; Bill, E.; Ye, S.; Deng, L. A Two-Coordinate Iron(II) Imido Complex with NHC Ligation: Synthesis, Characterization, and Its Diversified Reactivity of Nitrene Transfer and C-H Bond Activation. *Inorg. Chem.* **2019**, *58*, 7634-7644.
(48) Wang, Q.; Guo, J.; Chen, P. The Impact of Alkali and Alkaline Earth Metals on Green Ammonia Synthesis. *Chem* **2021**, *7*, 3203-3220.
(49) Cowley, R. E.; Holland, P. L. C–H Activation by a Terminal Imidoiron(III) Complex to Form a Cyclopentadienyliron(II) Product. *Inorg. Chim. Acta* **2011**, *369*, 40-44.
(50) King, E. R.; Hennessy, E. T.; Betley, T. A. Catalytic C-H Bond Amination From High-Spin Iron Imido Complexes. *J. Am. Chem. Soc.* **2011**, *133*, 4917-4923.
(51) Cowley, R. E.; Holland, P. L. Ligand Effects on Hydrogen Atom Transfer from Hydrocarbons to Three-Coordinate Iron Imides. *Inorg. Chem.* **2012**, *51*, 8352-8361.
(52) Hennessy, E. T.; Betley, T. A. Complex N-Heterocycle Synthesis via Iron-Catalyzed, Direct C–H Bond Amination. *Science* **2013**, *340*, 591-595.
(53) Iovan, D. A.; Betley, T. A. Characterization of Iron-Imido Species Relevant for N-Group Transfer Chemistry. *J. Am. Chem. Soc.* **2016**, *138*, 1983-1993.
(54) Spasyuk, D. M.; Carpenter, S. H.; Kefalidis, C. E.; Piers, W. E.; Neidig, M. L.; Maron, L. Facile Hdrogen Atom Transfer to Iron(III) Imido Radical Complexes Supported by a Dianionic Pentadentate Ligand. *Chem. Sci.* **2016**, *7*, 5939-5944.
(55) Wilding, M. J. T.; Iovan, D. A.; Betley, T. A. High-Spin Iron Imido Complexes Competent for C-H Bond Amination. *J. Am. Chem. Soc.* **2017**, *139*, 12043-12049.
(56) Wilding, M. J. T.; Iovan, D. A.; Wrobel, A. T.; Lukens, J. T.; MacMillan, S. N.; Lancaster, K. M.; Betley, T. A. Direct Comparison of C-H Bond Amination Efficacy through Manipulation of Nitrogen-Valence Centered Redox: Imido versus Iminyl. *J. Am. Chem. Soc.* **2017**, *139*, 14757-14766.
(57) Sridharan, A.; Brown, A. C.; Suess, D. L. M. A Terminal Imido Complex of an Iron-Sulfur Cluster. *Angew. Chem. Int. Ed.* **2021**, *60*, 12802-12806.
(58) Nieto, I.; Ding, F. Z.; Bontchev, R. P.; Wang, H. B.; Smith, J. M. Thermodynamics of Hydrogen Atom Transfer to a High-Valent Iron Imido Complex. *J. Am. Chem. Soc.* **2008**, *130*, 2716-2717.
(59) Liu, Q.; Long, L.; Ma, P.; Ma, Y.; Leng, X.; Xiao, J.; Chen, H.; Deng, L. Synthesis, Structure, and C–H Bond Activation Reaction of an Iron(IV) Terminal Imido Complex Bearing Trifluoromethyl Groups. *Cell Rep. Phys. Sci.* **2021**, *2*, 100454.
(60) Hong, S.; Sutherlin, K. D.; Vardhaman, A. K.; Yan, J. J.; Park, S.; Lee, Y. M.; Jang, S.; Lu, X.; Ohta, T.; Ogura, T.; Solomon, E. I.; Nam, W. A Mononuclear Nonheme Iron(V)-Imido Complex. *J. Am. Chem. Soc.* **2017**, *139*, 8800-8803.
(61) Brown, S. D.; Peters, J. C. Ground-State Singlet L_3Fe-(μ-N)-FeL_3 and $L_3Fe(NR)$ Complexes Featuring Pseudotetrahedral Fe(II) Centers. *J. Am. Chem. Soc.* **2005**, *127*, 1913-1923.
(62) Moret, M. E.; Peters, J. C. Terminal Iron Dinitrogen and Iron Imide Complexes Supported by a Tris(phosphino)borane Ligand. *Angew. Chem. Int. Ed.* **2011**, *50*, 2063-2067.
(63) Aldrich, K. E.; Fales, B. S.; Singh, A. K.; Staples, R. J.; Levine, B. G.; McCracken, J.; Smith, M. R., III; Odom, A. L. Electronic and Structural Comparisons between Iron(II/III) and Ruthenium(II/III) Imide Analogs. *Inorg. Chem.* **2019**, *58*, 11699-11715.
(64) Warren, J. J.; Tronic, T. A.; Mayer, J. M. Thermochemistry of Proton-Coupled Electron Transfer Reagents and its Implications. *Chem. Rev.* **2010**, *110*, 6961-7001.
(65) Rodriguez, M. M.; Stubbert, B. D.; Scarborough, C. C.; Brennessel, W. W.; Bill, E.; Holland, P. L. Isolation and Characterization of Stable Iron(I) Sulfide Complexes. *Angew. Chem. Int. Ed.* **2012**, *51*, 8247-8250.
(66) Ouyang, Z.; Du, J.; Wang, L.; Kneebone, J. L.; Neidig, M. L.; Deng, L. Linear and T-Shaped Iron(I) Complexes Supported by N-Heterocyclic Carbene Ligands: Synthesis and Structure Characterization. *Inorg. Chem.* **2015**, *54*, 8808-8816.
(67) Note that since model complexes were used for these calculations, the absolute BDFE values may differ from those for the real complexes. However, we expect the BDFE trend to be similar to that for the full complexes.
(68) Grubel, K.; Brennessel, W. W.; Mercado, B. Q.; Holland, P. L. Alkali Metal Control over N-N Cleavage in Iron Complexes. *J. Am. Chem. Soc.* **2014**, *136*, 16807-16816.
(69) Wicker, B. F.; Scott, J.; Andino, J. G.; Gao, X.; Park, H.; Pink, M.; Mindiola, D. J. Phosphinidene Complexes of Scandium: Powerful PAr Group-Transfer Vehicles to Organic and Inorganic Substrates. *J. Am. Chem. Soc.* **2010**, *132*, 3691-3693.

Table of Contents: